17th CIRP Conference on Modelling of Machining Operations

FEM modeling of hard turning 42CrMoS4 steel

M. Saez-de-Buruaga[a,*], L. Gainza[a], P. Aristimuno[a], D. Soler[a], G. Ortiz-de-Zarate[a],
O. Aizpuru[b], R. Mielgo[c], P.J. Arrazola[a]

aMondragon Unibertsitatea, Dpto. Mecanizado de Alto Rendimiento. Loramendi kalea 4, 20500, Mondragon, Gipuzkoa
bZUBIOLA S.Coop. Polígono Basterretxe, 44, 20720, Azkoitia, Gipuzkoa
cSHUTON S.A. Polígono Industrial Goiain, c/Subinoa 5, 01170, Legutio, Álava.

* Corresponding author. Tel.: +34 943794700; fax: + 34 943791536. *E-mail address:* msaez@mondragon.edu

Abstract

The aim of the present paper is to study by Finite Element Method (FEM) the hard turning of 42CrMoS4 steel. A numerical and experimental study was carried out to analyze the effect that cutting parameters have on cutting and feed forces, temperatures on the cutting zone, contact length and chip morphology. A flow stress model for the FEM model was developed by dynamic compression tests. Experimental tests were done to establish the accuracy of the FEM model, developed in DEFORM. The tendencies of both frameworks agreed in forces and temperatures. Greater differences were found for contact length and chip thickness predictions.

Keywords: Hard machining; FEM; Flow Stress.

1. Introduction

Hard turning is a topic of interest for the manufacturing and scientific communities. Quenched steels are widely used in the automotive industry, for the manufacturing of components such as gears, bearings, tools and dies. Traditionally, hardened steels have been machined by grinding. However, the grinding operations are slow and can only be used for specific geometrical shapes. Therefore, hard turning is a technological development that offers many potential benefits compared to grinding, which is still the standard finishing process for hardened steel surfaces [1]. Some decisive factors that lead to this process are the flexibility and ability to manufacture complex geometries, the reduction in cost and production time, the improved surface integrity and the reduction of coolants that harms the environment [2]. However, the main disadvantage of turning is the irregular spiral-shaped finish that is left in the piece, which sometimes requires another operation to correct it [3,4].

In the finishing operations, the increased hardness of the workpiece, in addition to the forces and temperatures in the contact area between the tool and workpiece, imply that the tool must be both rigid and resistant to wear. To solve this, Polycrystalline Cubic Boron Nitride (PCBN) tools have been proven viable for producing accurate hardened steel parts compared to carbide and coated ceramic tools [5].

In order to improve the fundamental understanding of hard turning and process optimization, the Finite Element Method (FEM) is becoming widely employed. It makes possible to predict the process of chip removal, in particular the cutting and feed forces, the temperatures in the cutting zone, the morphology of the chip and the contact length [6].

In this research, the modeling of the chip formation process has been carried out with DEFORM 2D commercial software, which is based on a Lagrangian formulation combined with automatic remeshing, in order to analyze the turning of 42CrMoS4 quenched-tempered hardened steel (60 HRC) using PCBN cutting tools. The objective of this study is to investigate

the influence that cutting speed and feed have on the main fundamental variables (cutting and feed forces, temperature in the cutting area, contact length and chip thickness) and compare them with experimental orthogonal cutting tests.

2. Finite Element modeling

In order to develop a reliable model, it is necessary to identify the input parameters as accurate as possible, as for example, the flow stress model, the material damage law and the friction law. All the parameters employed in the FE model are summarized in Table 1.

Table 1. Input parameters of the FEM model

Constitutive model	σ_s [MPa]	2505
	σ_0 [MPa]	2250
	A [MPa]	850
	n	0.924
	r	9.4
	m [K^{-1}]	0.01
	B [K]	565
	C	0.12
	$\dot{\varepsilon}_0$ [s^{-1}]	0.5
Young's modulus, E [GPa]	42CrMoS4	212 (20ºC)
		164 (600ºC)
	PCBN	900
Poisson's ratio, v	42CrMoS4	0.3
	PCBN	0.2
Density, ρ [kg/m³]	42CrMoS4	7850
	PCBN	3520
Conductivity, k [W/mºC]	42CrMoS4	41.7 (20ºC)
		34.1 (600ºC)
	PCBN	145
Expansion, λ [1/ºC]	42CrMoS4	1.19 e^{-5} (20ºC)
		1.49 e^{-5} (600ºC)
	PCBN	1.18 e^{-5}
Specific heat, c_p [J/kgºC]	42CrMoS4	460 (20ºC)
		777 (600 ºC)
	PCBN	457
Cockroft and Latham's material failure	D [MPa]	150
Friction coefficient	μ	0.35
	m	1
Friction energy to heat [%]		100
Inelastic heat fraction		0.9
Cutting speed, V_c [m/min]		160-180-200
Feed [mm]		0.01-0.055-0.1
Rake angle, γ [°]		0
Clearance angle, α [°]		5
Cutting edge radius, r [µm]		17

2.1. Flow stress model

The flow stress law for the 42CrMoS4 was obtained by dynamic and quasi-static compression tests at wide range of temperatures (20-680ºC) and strain rates (0.5-10s^{-1}). Test specimens were obtained from the outer diameter of the rolled bars, inside the 6-7 mm of induction-hardened section. The flow stress law (Eq. 1) consists of a strain hardening term (σ_ε), multiplied by dimensionless thermal softening (σ_T) and strain rate hardening terms ($\sigma_{\dot{\varepsilon}}$).

$$\sigma = \sigma_\varepsilon \cdot \sigma_T \cdot \sigma_{\dot{\varepsilon}} \tag{1}$$

In the proposed model, the strain hardening term was obtained from the research of [7], which is described in Eq. 2.

$$\sigma_\varepsilon = \sigma_s + (\sigma_0 - \sigma_s + A \cdot \varepsilon^n) \cdot \exp(-r \cdot \varepsilon) \tag{2}$$

where σ is the equivalent stress in MPa, σ_s the saturation stress (σ_s=2505MPa), σ_0 the yield stress (σ_s=2250MPa), A the strain hardening coefficient (A=850MPa), n the strain hardening exponent (n=0.924) and r the strain softening term (r=9.4).

Fig. 1 depicts the comparison between the modelled and the experimentally obtained flow stress behaviour at the conditions of 20ºC and 0.5s^{-1} strain rate.
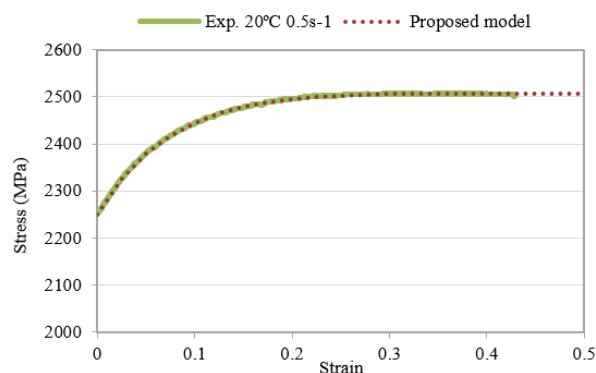

Fig. 1. Simulated and experimentally obtained flow stress curves at 20ºC and 0.01s-1 strain rate of the 42CrMoS4 steel

With regards to the thermal softening of the material, in the experimental tests a decrease in stress was observed when the temperature was increased, with a more noticeable stress drop at higher temperatures. Therefore, the experimental results were adjusted to the exponential term of Eq. 3 proposed by [8]. This equation considers the phenomenon of thermal softening as a non-linear function, which differs with the commonly employed Johnson and Cook model.

$$\sigma_\varepsilon = \frac{1}{1+e^{m(T-B)}} \tag{3}$$

Flow stress measured at temperature relative to flow stress at $T_0 = 20°C$ is plotted against temperature in Figure 2. The values of m=0.01ºC^{-1} and B=565ºC gave the best fit.
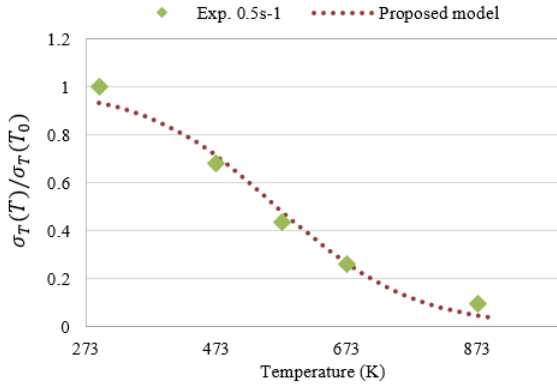
Fig. 2. Simulated and experimentally obtained flow stress curves at 20ºC and 0.5s⁻¹ strain rate of the 42CrMoS4 steel

The influence of the strain rate in the flow behavior was modelled with the equation proposed in the model of [9], Johnson and Cook (JC) model, and represented by Eq. 4.

$$\sigma_{\dot{\varepsilon}} = 1 + C \cdot \ln\left(\frac{\dot{\varepsilon}}{\dot{\varepsilon}_0}\right) \tag{4}$$

In the present case, as no data was accessible at the lower temperature range for the strain rates above 0.5s⁻¹, the parameters of Eq. 4 were obtained from the tests at 600ºC, in which was possible to characterize all the strain rate range. The value of C=0.12 gave the best fit for a reference strain rate of $\dot{\varepsilon}_0$=0.5s⁻¹ (see Fig. 3).
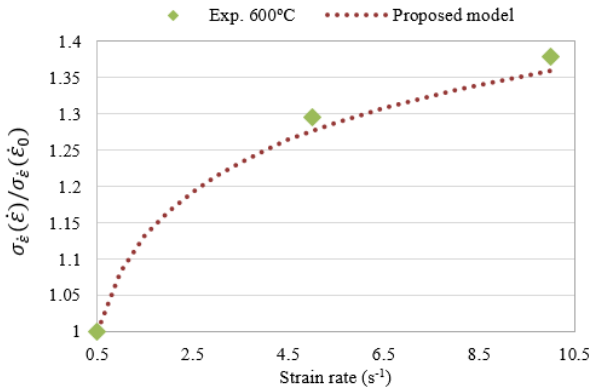

Fig. 3. Simulated and experimentally obtained flow stress curves at 600ºC and 0.5-5-10s⁻¹ strain rate of the 42CrMoS4 steel

2.2. Friction model

The influence that friction has on predicted results is known to be significant, as observed by Arrazola and Ozel [10]. For an accurate friction representation, this was modeled using the sticking-sliding model shown in Eq.5. The parameters were extracted from the publication of [11], in which the tempered material AISI 52100 was characterized by orthogonal cutting tests with PCBN tools. The values were μ=0.35 and m=1.

$$\tau = \min(\mu \cdot \sigma_n, m \cdot k) \tag{5}$$

where, τ is the friction stress, k is the yield stress in shear, σ_n the pressure at the interface and μ, m the friction parameters.

2.3. Damage model

For the prediction of the chip form and the fragile behavior of the material, a material failure was implemented in the FE code. In this case, the Cockroft and Latham damage criterion [12] was selected as the most suitable, according to which the fracture occurs when the accumulated stress state D reaches a critical damage value D_{cr}, as specified in Eq. 6.

$$D = \int_0^{\overline{\varepsilon}_f} \sigma_1 d\overline{\varepsilon} \tag{6}$$

where, $\overline{\varepsilon}_f$ is the effective fracture strain and σ_1 is the maximum principal stress. The material damage parameter D, of magnitude 150, was determined based on the data obtained by [13] and combined with an inverse simulation strategy in which the fundamental variables of the process were predicted as accurate as possible (cutting and feed forces, chip morphology and segmentation frequency).

2.4. Description of FE model

The commercial software DEFORM 2D, which uses a Lagrangian implicit code was used for the FEM modelling. The software provides robust results with a high control of the mesh.

The model consists of a rigid tool and an elastoplastic workpiece, meshed with 2500 and 7500 isoparametric quadrilateral elements respectively. The minimum element size was below 4 μm and the maximum was 8 μm. A local remeshing criteria based on strain and strain rate was established. The remeshing technique avoids mesh distortion at large strains, and allows maintaining small elements in the cutting area during computing.

The workpiece (0.5x2.5 mm) was fixed in space, and the tool moves horizontally from right to left at the cutting speed, to remove the upper layer of the workpiece. Fig. 4 shows all the boundary conditions applied to the model.

3. Orthogonal cutting tests

Experimental orthogonal cutting tests were carried out for the validation of the FEM model. For the measurement of output variables, the set-up detailed in previous publications was employed [14], and is schematically described in Fig. 5. The set-up is mounted on a CNC vertical milling machine. The tool holder together with the cutting insert are placed on a Kistler 9121 dynamometer to measure the cutting and feed forces, which is fixed to the moving table of the milling
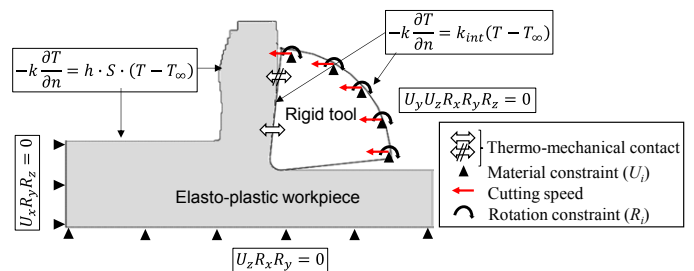

Fig. 4. Boundary conditions of the finite element model

machine. The set-up incorporates a infrared (IR) FLIR Titanium 550M camera to measure the temperature in the tool. The specimen, with cylindrical shape and 2 mm wall thickness (depth of cut), is placed in the spindle, allowing the rotation and vertical displacement, which corresponds to the cutting speed and feed, respectively.

One of the edges of the cutting inserts was ground (Fig. 5) to obtain a perpendicular surface for the IR measurements. In this way, it is possible to capture the thermal field on one side of the tool. The IR camera captures the radiation emitted by the tool, measured in Digital Levels (DL). To obtain the real temperature of the surface, the relation of DL-temperature was calibrated by the method described in [15]. This methodology consists on the simultaneous recording of the radiated temperature (measured in DL by the IR camera) and the real temperature of the measured surface with two thermocouples. In this way, the characterization of the emissivity is avoided, and a DL-temperature function that inherently includes the effect of the emissivity is extracted. The main advantage is that the characterization is done in conditions identical to those during the orthogonal cutting tests (optical path, field of view). Finally, as described in [16], the experimental temperature measurements were extrapolated from the ground surface on the side of the tool to the mid plane of the contact zone between tool and chip. This is done analytically based on the theories of heat generation in cutting processes and the transfer of heat inside the volume of a semi-infinite solid.

The tests were carried out in five cutting conditions using cutting speeds (V_c) of 160, 180 and 200 m/min, and feedrates (A_v) of 0.01, 0.055 and 0.1 mm/rev. For each trial a minimum of three repetitions were made. PCBN inserts (with 85% CBN content) were used with a clearance angle of 5º, rake angle of 0º, edge radius of 17µm and chamfer of 0.14x14º. In each tested condition, a new insert was used to prevent the results of being affected by tool wear, and for the subsequent measurement of the contact lengths. Chips were also collected for the analysis of chip morphology.

4. Analysis of results

The following fundamental variables were analyzed in both experimental and numerical frameworks: cutting and feed forces, temperature of the tool/chip contact section, chip morphology and tool/chip contact length. In the modeling
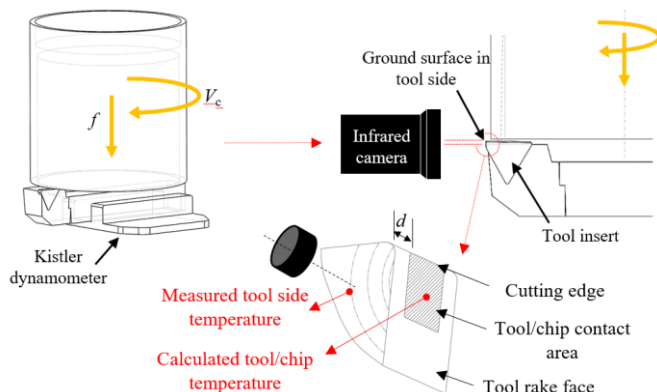
section, the simulation time oscillates between 20-27h for the analyzed cutting conditions, and it is worth noting that the analysis was done once the thermal steady state was reached.

4.1. Cutting and feed forces

In the analysis of the cutting forces the same trend was observed in both experimental and numerical fields (see Fig. 6). An increase in cutting forces with the increase in feed was observed in the tested feed range. The decrease in the cutting forces together with the increase in cutting speed occurred also, except for the case of lower feed. At this feed of 0.01mm/rev, the cutting force increased with the increase in cutting speed in both experiments and simulations. The magnitudes obtained by the numerical model were close to those of the experimental results, within an average error of 10%. The condition with the feed of 0.01 mm/rev was that with the highest deviation, approximately 18%, while at the highest feed the maximum error was a 2%.

Focusing on the feed forces, these also increased together with the feed, and decreased with the cutting speed except at the feed of 0.01mm/rev (see Fig. 6). At this feed, an increase in forces occurred when the cutting speed was increased. The trends matched when both numerical and experimental results were compared. Analyzing the magnitudes, however, greater differences were observed between the two frameworks than those found in the cutting forces. The greatest occurred at the feed of 0.01 mm/rev. This may be related to the effect that the cutting edge radius has on the feed force component, as at that condition the cutting edge radius is larger than the feed (0.017mm versus 0.01mm/rev feed). Therefore, in the experimentally measured forces there is a component related to the ploughing effect that might not be correctly represented in the model. This could be attributed to a friction behavior not properly modeled in the vicinities of the cutting edge of the tool. In spite of these differences, when cutting with feeds of 0.055 and 0.1 mm/rev, the predicted magnitudes approached the experimental ones with an average error of 7%.
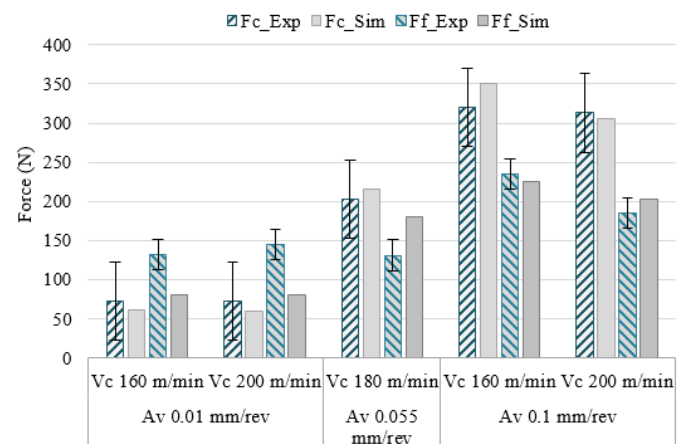

Fig. 6. Comparison of cutting and feed forces between the experiments and simulations

Fig. 5. Scheme of the setup for orthogonal cutting and IR temperature measurement

4.2. Tool/chip contact temperatures

Fig. 7-a shows an example of a thermal field which has been measured in the tool side and then has been recalculated to that of the tool/chip contact. This can be compared with the thermal field of the FE model in Fig. 7-b.

The predicted and experimental magnitudes of the maximum temperatures in the tool/chip contact are plotted in Fig. 8. As described in the methodology, an analytical model was applied to extrapolate the experimentally measured temperature on the side face of the tool to the cutting zone [15]. This model is only applicable when the feed is greater than the cutting edge radius, as the analytical theories were developed considering sharp cutting edges. Therefore, in the case of the feed of 0.01 mm/rev, it was not reasonable to calculate the tool/chip temperatures since the edge radius of the inserts was 0.017 mm (see Fig. 7).

From Fig. 7 and focusing on the trends of the simulations, it is possible to observe that the temperatures increased with both the feed and cutting speed. In turn, experimentally no remarkable differences were found between the analyzed cutting conditions. Only, it could be guessed that and slight temperature increase occurred when the cutting speed was increased, but not clear conclusions could be extracted concerning the effect of the feed. The differences in magnitude between obtained an average error of 9%.

4.3. Tool/chip contact length

The predicted contact lengths (l_c) in the model followed the trend of the experiments. The expected increase in l_c with the increase in feed was correctly modelled. Of further
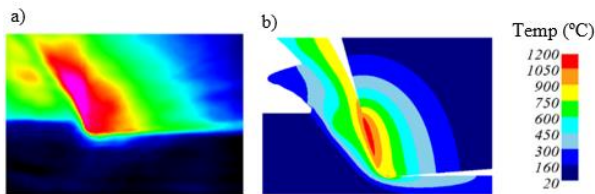

Fig. 7. Experimental (a) and simulated (b) thermal fields when cutting at V_c=160m/min and A_v=0,1mm/rev
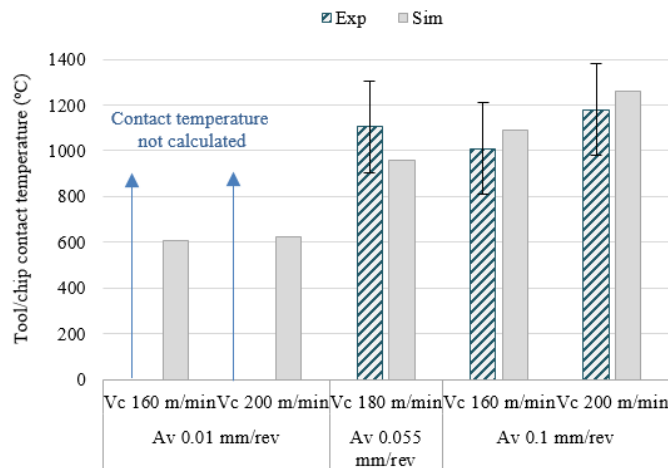

Fig. 8. Comparison of tool/chip contact temperatures between the experiments and simulations

interest is the almost no influence that cutting speed had at the feed of 0.01mm/rev, while at the feed of 0.1 mm/rev the increase in cutting speed caused an increase in contact length (Fig. 9). The magnitudes, however, were underestimated in all conditions with an average error of 29%, being the predictions at the feed of 0.01 mm/rev those with the greatest deviation. Again, this may be related to the fact that friction was not characterized for the selected tool-workpiece material pair in this research, and instead the friction parameters were taken from a hardened AISI 52100 steel.
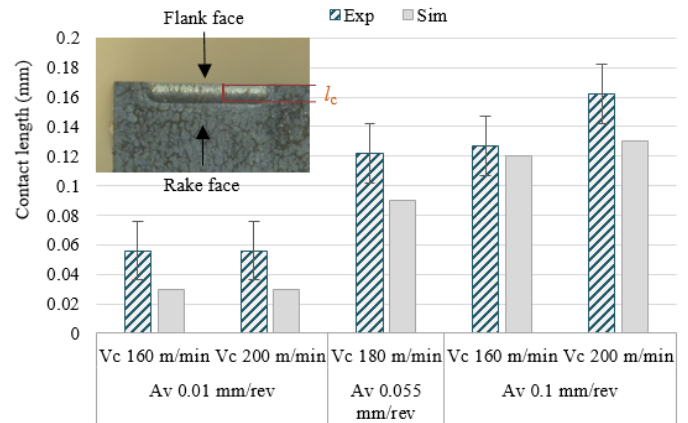

Fig. 9. Comparison of tool/chip contact lengths between the experiments and simulations

4.4. Chip thickness and chip morphology

The peaks, valleys and distance between peaks (pitch) were measured for each cutting condition. In general, this were predicted accurately. As observed in Fig. 10, in the cases of greater feed the chip was segmented (Fig. 10-a), while with feeds of 0.01 mm/rev this was continuous (Fig. 10-b). These morphologies coincided in both the experimental tests and in the simulation results. In addition, it could be observed that the strain distribution was coherent, obtaining higher strain values in the valleys.

Although the trends of the simulations matched those of the experiments, the estimated magnitudes had some deviations depending on the analyzed condition (see Fig. 11). Specifically, the experimental peak/valley ratio was very high in the tests at feeds of 0.1 mm/rev, while in the simulations this relationship was considerably lower. These deviations could be related to the damage model, which could be re-adjusted.
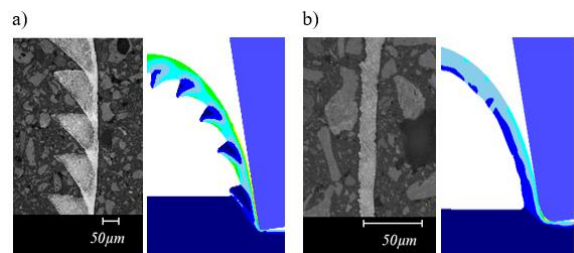

Fig. 10. Comparison of chip morphology when cutting at (a) Vc=160m/min-Av=0.1mm/rev and (b) Vc=160m/min and Av=0.01mm/rev
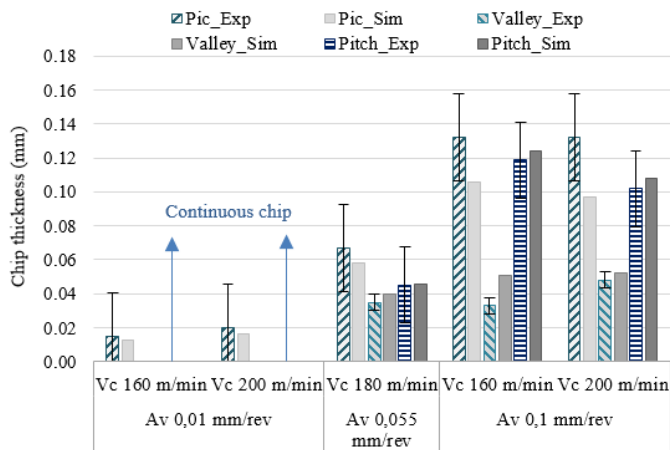
Fig. 11. Scheme of the setup for orthogonal cutting and IR temperature measurement

5. Conclusions

A numerical model capable of predicting the forces, temperatures, contact lengths and chip morphology that represents the experimental trends observed in orthogonal cutting tests was developed. This shows the capabilities of FEM modeling to analyze the hard turning process. The conclusions reached are the following:

- A rheological analysis of the hardened 42CrMoS4 steel was carried out in order to characterize the behavior at high temperatures and strain rates. These tests permitted to characterize a flow stress law that differs from the widely used Johnson-Cook law. The model is able to reflect the non-linear thermal softening and models with a high degree of accuracy the strain hardening of the material.
- The cutting forces of the simulations were comparable to the experimental results in both trends and magnitudes, achieving an average error of 10%.
- The trends of the feed forces were accurate at the higher feeds and the predictions showed an error of less than 10%. In the tests with feeds of 0.01 mm/rev, the feed forces were under predicted compared to the experimental values. This could be linked to the effect of the ploughing forces occurred when cutting at feeds lower than the cutting edge radius, which were not correctly modeled. An improved friction law could help to solve this issue.
- The prediction of temperatures at the high feeds were found close in magnitude. However, it was not possible to extrapolate the temperatures in the cutting zone for the experimental tests at feeds of 0.01 mm/rev and, therefore, the accuracy of the temperature estimates at this condition are unknown.
- The values of the predicted contact lengths were lower than the measured experimental values, although results followed the same trends in all the cutting conditions. However, the contact length was the variable with the highest estimation error, which could be linked to the modeled friction behavior.
- The chip morphology was satisfactorily predicted. The trends of the measurements coincided with the experiments, although slight variations occurred in the distance between peaks and valleys.

References

[1] Tönshoff, H. K., Arendt, C., & Amor, R. B. (2000). Cutting of hardened steel. CIRP Annals-Manufacturing Technology, 49(2), 547-566.

[2] Klocke, F., Brinksmeier, E., & Weinert, K. (2005). Capability profile of hard cutting and grinding processes. CIRP Annals-Manufacturing Technology, 54(2), 22-45.

[3] Hammerström, L., & Jacobson, S. (2006). Surface modification of brake discs to reduce squeal problems. Wear, 261(1), 53-57.

[4] Rodríguez, A., de Lacalle, L. N. L., Fernández, A., & Braun, S. (2014). Elimination of surface spiral pattern on brake discs. Journal of Zhejiang University SCIENCE A, 15(1), 53-60.

[5] Chinchanikar, S., & Choudhury, S. K. (2015). Machining of hardened steel—experimental investigations, performance modeling and cooling techniques: a review. International Journal of Machine Tools and Manufacture, 89, 95-109.

[6] Arrazola, P. J., Özel, T., Umbrello, D., Davies, M., & Jawahir, I. S. (2013). Recent advances in modelling of metal machining processes. CIRP Annals, 62(2), 695-718.

[7] Lurdos, O., Montheillet, F., & Damamme, G. (2008). Empirical and physically based flow rules relevant to high speed processing of 304L steel. International Journal of Material Forming, 1(1), 1431-1434.

[8] Iturbe, A., Giraud, E., Hormaetxe, E., Garay, A., Germain, G., Ostolaza, K., & Arrazola, P. J. (2017). Mechanical characterization and modelling of Inconel 718 material behavior for machining process assessment. Materials Science and Engineering: A, 682, 441-453.

[9] Johnson, G. R., & Cook, W. H. (1985). Fracture characteristics of three metals subjected to various strains, strain rates, temperatures and pressures. Engineering fracture mechanics, 21(1), 31-48.

[10] Arrazola, P. J. (2010). Investigations on the effects of friction modeling in finite element simulation of machining. International journal of mechanical sciences, 52(1), 31-42.

[11] Guo, Y. B., & Liu, C. R. (2002). 3D FEA modeling of hard turning. Journal of manufacturing science and engineering, 124(2), 189-199.

[12] Cockcroft, M. G., & Latham, D. J. (1968). Ductility and the workability of metals. J Inst Metals, 96(1), 33-39.

[13] Umbrello, D. (2008). Finite element simulation of conventional and high speed machining of Ti6Al4V alloy. Journal of materials processing technology, 196(1-3), 79-87.

[14] Arrazola, P. J., Aristimuno, P., Soler, D., & Childs, T. (2015). Metal cutting experiments and modelling for improved determination of chip/tool contact temperature by infrared thermography. CIRP Annals, 64(1), 57-60.

[15] Soler, D., Aristimuño, P. X., Saez-de-Buruaga, M., Garay, A., & Arrazola, P. J. (2018). New calibration method to measure rake face temperature of the tool during dry orthogonal cutting using thermography. Applied Thermal Engineering, 137, 74-82.

[16] Saez-de-Buruaga, M., Soler, D., Aristimuño, P. X., Esnaola, J. A., & Arrazola, P. J. (2018). Determining tool/chip temperatures from thermography measurements in metal cutting. Applied Thermal Engineering, 145, 305-314.